New Constraint on the Local Relic Neutrino Background Overdensity with the First KATRIN Data Runs

M. Aker,[1] D. Batzler,[1] A. Beglarian,[2] J. Behrens,[3] A. Berlev,[4] U. Besserer,[1] B. Bieringer,[5] F. Block,[6] S. Bobien,[7] B. Bornschein,[1] L. Bornschein,[3] M. Böttcher,[5] T. Brunst,[8, 9] T. S. Caldwell,[10, 11] R. M. D. Carney,[12] S. Chilingaryan,[2] W. Choi,[6] K. Debowski,[13] M. Descher,[6] D. Díaz Barrero,[14] P. J. Doe,[15] O. Dragoun,[16] G. Drexlin,[6] F. Edzards,[8, 9] K. Eitel,[3] E. Ellinger,[13] R. Engel,[3] S. Enomoto,[15] A. Felden,[3] J. A. Formaggio,[17] F. M. Fränkle,[3] G. B. Franklin,[18] F. Friedel,[3] A. Fulst,[5] K. Gauda,[5] A. S. Gavin,[10, 11] W. Gil,[3] F. Glück,[3] R. Grössle,[1] R. Gumbsheimer,[3] V. Hannen,[5] N. Haußmann,[13] K. Helbing,[13] S. Hickford,[3] R. Hiller,[3] D. Hilesheimer,[1] D. Hinz,[3] T. Höhn,[3] T. Houdy,[8, 9] A. Huber,[3] A. Jansen,[3] C. Karl,[8, 9] F. Kellerer,[9, *] J. Kellerer,[6] M. Kleifges,[2] M. Klein,[3] C. Köhler,[8, 9] L. Köllenberger,[3] A. Kopmann,[2] M. Korzeczek,[6] A. Kovalík,[16] B. Krasch,[1] H. Krause,[3] L. La Cascio,[6] T. Lasserre,[19, *] T. L. Le,[1] O. Lebeda,[16] B. Lehnert,[12] A. Lokhov,[5, 4] M. Machatschek,[3] E. Malcherek,[3] M. Mark,[3] A. Marsteller,[1] E. L. Martin,[10, 11] C. Melzer,[1] S. Mertens,[8, 9] J. Mostafa,[2] K. Müller,[3] H. Neumann,[7] S. Niemes,[1] P. Oelpmann,[5] D. S. Parno,[18] A. W. P. Poon,[12] J. M. L. Poyato,[14] F. Priester,[1] J. Rális,[16] S. Ramachandran,[13] R. G. H. Robertson,[15] W. Rodejohann,[20] C. Rodenbeck,[5] M. Röllig,[1] C. Röttele,[1] M. Ryšavý,[16] R. Sack,[3, 5] A. Saenz,[21] R. Salomon,[5] P. Schäfer,[1] L. Schimpf,[5, 6] M. Schlösser,[1] K. Schlösser,[3] L. Schlüter,[8, 9] S. Schneidewind,[5] M. Schrank,[3] A. Schwemmer,[8, 9] M. Šefčík,[16] V. Sibille,[17] D. Siegmann,[8, 9] M. Slezák,[8, 9] F. Spanier,[22] M. Steidl,[3] M. Sturm,[1] H. H. Telle,[14] L. A. Thorne,[23] T. Thümmler,[3] N. Titov,[4] I. Tkachev,[4] K. Urban,[8, 9] K. Valerius,[3] D. Vénos,[16] A. P. Vizcaya Hernández,[18] C. Weinheimer,[5] S. Welte,[1] J. Wendel,[1] C. Wiesinger,[8, 9] J. F. Wilkerson,[10, 11] J. Wolf,[6] S. Wüstling,[2] J. Wydra,[1] W. Xu,[17] S. Zadoroghny,[4] and G. Zeller[1]

(KATRIN Collaboration)

[1]*Tritium Laboratory Karlsruhe (TLK), Karlsruhe Institute of Technology (KIT),
Hermann-von-Helmholtz-Platz 1, 76344 Eggenstein-Leopoldshafen, Germany*
[2]*Institute for Data Processing and Electronics (IPE), Karlsruhe Institute of
Technology (KIT), Hermann-von-Helmholtz-Platz 1, 76344 Eggenstein-Leopoldshafen, Germany*
[3]*Institute for Astroparticle Physics (IAP), Karlsruhe Institute of Technology (KIT),
Hermann-von-Helmholtz-Platz 1, 76344 Eggenstein-Leopoldshafen, Germany*
[4]*Institute for Nuclear Research of Russian Academy of Sciences, 60th October Anniversary Prospect 7a, 117312 Moscow, Russia*
[5]*Institute for Nuclear Physics, University of Münster, Wilhelm-Klemm-Str. 9, 48149 Münster, Germany*
[6]*Institute of Experimental Particle Physics (ETP), Karlsruhe Institute of
Technology (KIT), Wolfgang-Gaede-Str. 1, 76131 Karlsruhe, Germany*
[7]*Institute for Technical Physics (ITEP), Karlsruhe Institute of Technology (KIT),
Hermann-von-Helmholtz-Platz 1, 76344 Eggenstein-Leopoldshafen, Germany*
[8]*Technische Universität München, James-Franck-Str. 1, 85748 Garching, Germany*
[9]*Max-Planck-Institut für Physik, Föhringer Ring 6, 80805 München, Germany*
[10]*Department of Physics and Astronomy, University of North Carolina, Chapel Hill, NC 27599, USA*
[11]*Triangle Universities Nuclear Laboratory, Durham, NC 27708, USA*
[12]*Institute for Nuclear and Particle Astrophysics and Nuclear Science
Division, Lawrence Berkeley National Laboratory, Berkeley, CA 94720, USA*
[13]*Department of Physics, Faculty of Mathematics and Natural Sciences,
University of Wuppertal, Gaußstr. 20, 42119 Wuppertal, Germany*
[14]*Departamento de Química Física Aplicada, Universidad Autonoma de Madrid, Campus de Cantoblanco, 28049 Madrid, Spain*
[15]*Center for Experimental Nuclear Physics and Astrophysics, and
Dept. of Physics, University of Washington, Seattle, WA 98195, USA*
[16]*Nuclear Physics Institute, Czech Academy of Sciences, 25068 Řež, Czech Republic*
[17]*Laboratory for Nuclear Science, Massachusetts Institute of Technology, 77 Massachusetts Ave, Cambridge, MA 02139, USA*
[18]*Department of Physics, Carnegie Mellon University, Pittsburgh, PA 15213, USA*
[19]*IRFU (DPhP & APC), CEA, Université Paris-Saclay, 91191 Gif-sur-Yvette, France*
[20]*Max-Planck-Institut für Kernphysik, Saupfercheckweg 1, 69117 Heidelberg, Germany*
[21]*Institut für Physik, Humboldt-Universität zu Berlin, Newtonstr. 15, 12489 Berlin, Germany*
[22]*Institute for Theoretical Astrophysics, University of Heidelberg, Albert-Ueberle-Str. 2, 69120 Heidelberg, Germany*
[23]*Institut für Physik, Johannes-Gutenberg-Universität Mainz, 55099 Mainz, Germany*
(Dated: February 10, 2022)

We report on the direct cosmic relic neutrino background search from the first two science runs of the KATRIN experiment in 2019. Beta-decay electrons from a high-purity molecular tritium gas source are analyzed by a high-resolution MAC-E filter around the kinematic endpoint at 18.57 keV. The analysis is sensitive to a local relic neutrino overdensity of $\eta = 9.7 \cdot 10^{10}$ ($1.1 \cdot 10^{11}$) at a 90% (95%) confidence level. A fit of the integrated electron spectrum over a narrow interval around the kinematic endpoint accounting for relic neutrino captures in the tritium source reveals no significant

overdensity. This work improves the results obtained by the previous kinematic neutrino mass experiments at Los Alamos and Troitsk. We furthermore update the projected final sensitivity of the KATRIN experiment to $\eta < 1 \cdot 10^{10}$ at 90% confidence level, by relying on updated operational conditions.

Introduction – In modern cosmology, neutrinos decoupled from the other particles of the standard model when the universe was about one second old. The existence of a cosmic (or relic) neutrino background (CνB) is predicted with great confidence. A direct measurement of CνB remains one of the most difficult tasks in neutrino physics and would yield direct information about the early history of the universe. Theoretical predictions of the local relic neutrino overdensity (η) range from 1.2 to 20 for neutrino masses below 0.6 eV, depending on the neutrino mass and the assumed density profile of the Milky Way [1, 2]. Relic neutrinos can interact with radioactive nuclei, like tritium, via the neutrino capture reaction $\nu_e + N_Z^A \longrightarrow N_{Z+1}^A + e^-$ [3, 4]. On this basis, previous kinematic neutrino mass experiments have provided upper bounds on the local overdensity η of relic neutrinos (with respect to the average across the universe of 56 cm^{-3} per species [1]) of $1 \cdot 10^{13}$ [5, 6]. Using a similar but extensively improved technology, the Karlsruhe Tritium Neutrino Experiment (KATRIN), shown in figure 1, provides a high-precision measurement of the electron spectrum of the tritium β-decay, ^{3}H $\rightarrow$ ^{3}He$^+$ + e$^-$ + $\overline{\nu}_e$ (endpoint $E_0 = 18.57$ keV, half-life $t_{1/2} = 12.32$ yr). Primarily operated to measure the effective neutrino mass m_ν, KATRIN already holds an upper limit of $m_\nu < 0.8$ eV at 90% confidence level [7] following the first two science runs in 2019. Using the same data set [7–9], we establish new constraints on the local overdensity of relic neutrinos.

Experimental setup – KATRIN combines a windowless gaseous molecular tritium source (WGTS) [6], with two spectrometers based on the principle of magnetic adiabatic collimation with electrostatic filtering (MAC-E-filter) [10–13]. Figure 1 displays the 70 m long experimental setup located at the Karlsruhe Institute of Technology (KIT) in Germany.

Source-related components in contact with tritium, shown in figure 1 a-c, are part of the Tritium Laboratory Karlsruhe to enable a closed cycle of tritium [14]. High-purity tritium gas is continuously injected into the WGTS at 30 K. The gas diffuses from the center to the ends of the WGTS where it is pumped out by several turbomolecular pumps and a cryotrap in the pumping section (figure 1 c). This reduces the flow rate of tritium into the spectrometer and detector sections (figure 1 d-f) by more than 14 orders of magnitude to suppress source-related background [15, 16]. In the spectrometer section, using the MAC-E-filter technique, electrons of charge q are guided by the magnetic field and precisely filtered by

———————
* Corresponding authors:
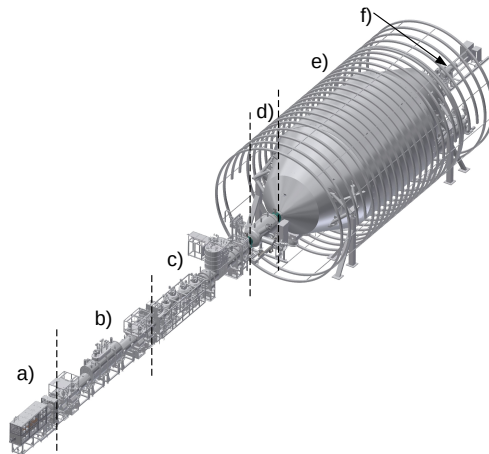kellerer@mpp.mpg.de and thierry.lasserre@cea.fr

FIG. 1. The main components of KATRIN: a) the rear Section, b) the windowless gaseous tritium source WGTS, c) the pumping section, and a tandem set-up of two MAC-E- filters: d) the smaller pre-spectrometer and e) the larger main spectrometer with surrounding aircoil system. This setup allows only the highest energy β-decay electrons to reach the focal plane detector f) where they are counted.

an electrostatic barrier (retarding energy qU). Only electrons whose energy is sufficient to overcome this barrier are transmitted to the focal plane detector (figure 1 f). By varying the High Voltage (HV) setting U, the tritium β-decay spectrum is measured in an integral mode, with an energy resolution of $\Delta E = 2.8$ eV at E_0. Transmitted electrons are subsequently counted, as a function of qU, by the focal plane silicon detector, segmented in 148 pixels [17]. Details and performance of the KATRIN setup, specified in [18], are reported in [14, 16, 19, 20].

First measurement campaign (KNM1) – The first science run was carried out from April 10 to May 13, 2019. All experimental details were already reported in [8]. The average source activity was $2.45 \cdot 10^{10}$ Bq (3.4 µg of tritium) at a column density of $1.11 \cdot 10^{17}$ molecules cm^{-2}, corresponding to about 20% of its nominal value. The integral tritium β-decay spectrum was scanned continuously in a range of [E_0-91 eV, E_0+49 eV] over a series of non-equidistant HV settings of the spectrometer electrode system. At each HV set point, the number of transmitted electrons is measured. In this search for relic neutrinos, we analyze the region from 37 eV below E_0 (22 HV set points) to 49 eV above (5 HV set points), as shown in the measurement time distribution (MTD) in figure 2 (bottom). We first merge the 117 best detector pixels into a single unique effective pixel. Quality cuts in the slow control parameters associated with each tritium scan shorten our data set to 274 stable scans for an over-

all scan time of 521.7 h. The good timing stability and reproducibility of the HV set points allowed us to stack the data of the 274 scans into a single spectrum, which is displayed in figure 2 (top) in units of counts per second (cps) [8]. This stacked integral spectrum, $R(\langle qU \rangle)$, includes $1.48 \cdot 10^6$ β-decay electrons expected below E_0. The background (292 mcps) originates mainly from the spectrometer and has two primary sources. A significant part is contributed by the thermal ionization of Rydberg atoms that sputter off the inner spectrometer surfaces by ^{206}Pb-recoil ions following α-decays of ^{210}Po. Another source of background are secondary electrons induced by α-decays of single ^{219}Rn atoms emanating from the vacuum pumps of the large spectrometer [21]. These electrons start at sub-eV energies, but are later accelerated to qU by the MAC-E-filter. The radon-induced background also causes a small non-Poissonian rate over-dispersion increasing the background statistical uncertainty (see [8] for details).
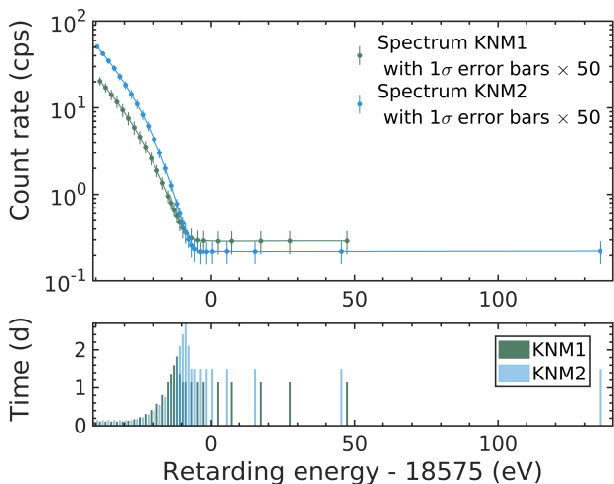

FIG. 2. Uniform electron spectra $R(\langle qU \rangle)$ of both data sets, with 1-σ error enlarged by factor 50. The blue and gray lines represent the β-decay best-fit models $R_{\beta,\text{calc}}(\langle qU \rangle)$. Above E_0, we see a flat background R_{bg} (top). Integral measurement time distributions of both data sets (bottom).

Second measurement campaign (KNM2) – The second measurement campaign was conducted from September 27 to November 19, 2019. The tritium source was operated at its nominal activity of $9.5 \cdot 10^{10}$ Bq (13.0 µg of tritium), yielding more than twice the number of β-decay electrons in the analysis range from E_0-40 eV to E_0 at $3.68 \cdot 10^6$ [7] as for the KNM1 cycle. To better assess the background, the analysis interval was extended to $[E_0$-40 eV, E_0+135 eV]. Improved vacuum conditions enabled a 25% reduction of the spectrometer background compared to KNM1 [22]. The KNM2 science run led to the collection of a data set of 361 stable scans with an overall scan time of 743.7 h that were combined into an effective single spectrum after gathering the 117 best pixels [7].

Modeling – The modeled experimental spectrum $R_{\text{calc}}(\langle qU \rangle)$ is calculated by convolving the expected differential spectrum of the signal $R_{\text{diff}}(E)$ with the calculated response function $f(E - \langle qU \rangle)$, in addition to the qU-independent background rate R_{bg}:

$$R_{\text{calc}}(\langle qU \rangle) = \int_{qU}^{E_0} R_{\text{diff}}(E) \cdot f(E - \langle qU \rangle) \, dE$$
$$+ R_{\text{bg}} \quad (1)$$

The response function $f(E - \langle qU \rangle)$ gives the transmission probability of an electron as a function of its surplus energy $E - \langle qU \rangle$. It includes the angular spread of electrons and their probability to undergo inelastic scattering processes (see [8] for details). Accounting for the relic neutrinos, the differential spectrum $R_{\text{diff}}(E)$ is the sum of the β-decay and neutrino-capture differential spectra, $R_\beta(E)$ and $R_{\text{C}\nu\text{B}}(E)$ respectively:

$$R_{\text{diff}}(E) = R_\beta(E) + R_{\text{C}\nu\text{B}}(E). \quad (2)$$

The differential spectrum $R_\beta(E)$ from the super-allowed β-decay of molecular tritium is given by:

$$R_\beta(E) = A_{\text{s}} \cdot N_{\text{T}} \cdot \frac{G_{\text{F}}^2 \cdot \cos^2\Theta_{\text{C}}}{2\pi^3} \cdot |M_{\text{nucl}}^2|$$
$$\cdot F(E, Z') \cdot (E + m_{\text{e}}) \cdot \sqrt{(E + m_{\text{e}})^2 - m_{\text{e}}^2}$$
$$\cdot \sum_j \zeta_j \cdot \epsilon_j \cdot \sqrt{\epsilon_j^2 - m_\nu^2} \cdot \Theta(\epsilon_j - m_\nu) \quad (3)$$

Equation 3 contains the square of the nuclear matrix element $|M_{\text{nucl}}^2|$, the neutrino kinetic energy $\epsilon_j = E_0 - E - V_j$, the Fermi constant G_{F}, the Cabibbo angle Θ_{C}, the electron mass m_{e}, and the Fermi function $F(E, Z' = 2)$. A_{s} is the normalization of the tritium β-decay, and N_{T} denotes the number of tritium atoms in the source multiplied with the solid angle of the setup $\Delta\Omega/4\pi = (1 - \cos\theta_{\text{max}})/2$, with $\theta_{\text{max}} = 50.5°$, and the detector efficiency of 0.95. The calculation of $R_\beta(E)$ involves a sum over a molecular final-state distribution (FSD), which describes the probabilities ζ_j with which the daughter ion ^{3}HeT$^+$ is left in a rotational, vibrational, and/or electronic state with excitation energy V_j added to the daughter molecule recoil, as described in [8]. Finally, our calculations include radiative corrections and the thermal Doppler broadening due to the motions of the tritium molecules in the WGTS [23].

Relic neutrino analysis – Relic neutrinos have a negligible $\mathcal{O}$(meV) kinetic energy compared to the energy released in the neutrino capture reaction on tritium. The differential neutrino capture spectrum is therefore given by the convolution of a Dirac delta function at $E_0 + 2m_\nu$ with the FSD. The mean excitation energies of the FSD are given relative to the ro-vibrational ground state of ^{3}HeT$^+$ and include the recoil energy for ^{3}HeT$^+$ [24]. Electronic excited states are involved in 43 % of neutrino

captures that shift part of the neutrino capture signal well below the endpoint (Fig. 3), where it is buried by the prominent β-decay background. These captures are therefore neglected in what follows. The remaining signal reflects captures involving the molecular ro-vibrational states, which are the same, to a good approximation, for β-decay and neutrino capture [25]. We further simplify by modeling the ro-vibrational and the Doppler broadenings by a 0.4 eV-wide Gaussian distribution. Simulations confirm that this proxy has no substantial impact on our results.
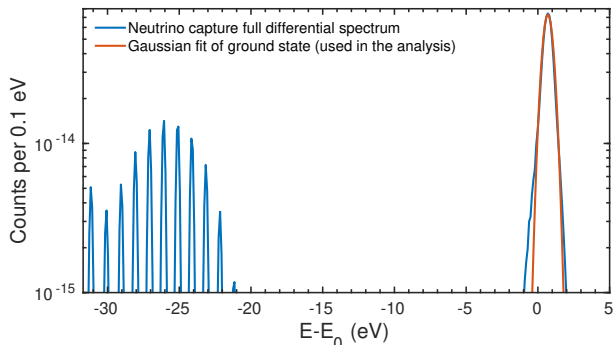

FIG. 3. Relic neutrino differential signal with arbitrary exposure, full model (blue) and Gaussian simplified model (red) for $\eta = 1$ and $m_\nu = 0.7$ eV.

The neutrino capture differential spectrum is then:

$$R_{\mathrm{C\nu B}}(E) = \frac{\eta \cdot N_{\mathrm{T}} \cdot \epsilon_{\mathrm{FSD}} \cdot R_{\mathrm{cap}} \cdot T}{\sqrt{2\pi\sigma_{\mathrm{C\nu B}}^2}}$$
$$\cdot \exp\left(-\frac{(E - E_0 - m_\nu + \langle E_{\mathrm{GS}}\rangle)^2}{2\sigma_{\mathrm{C\nu B}}^2}\right), \quad (4)$$

where η denotes the local relic neutrino overdensity, ϵ_{FSD} the ground-state fraction of the FSD, $R_{\mathrm{cap}} = 4.2 \cdot 10^{-25}$ yr^{-1} the relic neutrino capture rate on a single tritium nucleus for Majorana neutrinos [26], and T the measurement time. For Dirac neutrinos in the non-relativistic limit, R_{cap} is halved [26]. The final values quoted in this work are given for Majorana neutrinos.

In the case of molecular tritium, the endpoint of the β decay spectrum is broadened by the FSD ground state, and effectively extended by the mean ground state energy $\langle E_{\mathrm{GS}}\rangle \approx 1.7$ eV, which is equal to the recoil energy of a tritium molecule at the endpoint. This is due to the extended distribution of the FSD ground state, which includes a small fraction of β-decay electrons that only loose a minor amount of energy to molecular excitations. This leads to an irreducible background of the relic neutrino signal for neutrino masses smaller than $\langle E_{\mathrm{GS}}\rangle/2 = 0.85$ eV, as the CνB signal overlaps with the β-decay spectrum tail. Figure 4 illustrates this situation for $\eta = 1$. The β spectrum with molecular tritium (yellow) is extended by a high-energy tail compared to the β spectrum without FSD smearing (blue), and exceeds the CνB signal (purple) by about 7 orders of magnitude.
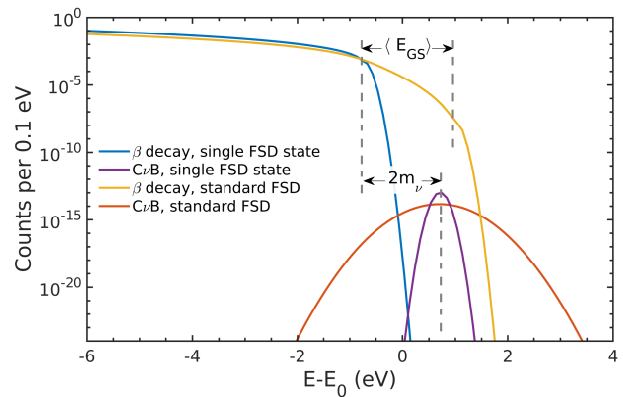

FIG. 4. Simulated impact of the molecular effects (FSD) on the β-decay and neutrino capture differential spectra of molecular tritium, for $\eta = 1$ and $m_\nu = 0.7$ eV (arbitrary exposure). All spectra also include Doppler broadening.

This ratio can only be improved by an increased CνB overdensity. In view of the above considerations, and as discussed in [27], it seems unlikely that any experiment using a molecular tritium source could achieve η limits well below $1 \cdot 10^6$ for neutrino masses below 0.85 eV, making the actual detection of CνB with molecular tritium virtually impossible.

Finally, in our analysis we only allow the neutrino mass squared to be positive, for two reasons: First, the average energy of the neutrino capture signal $E_{\mathrm{C\nu B}} = E_0 + 2m_\nu - \langle E_{\mathrm{GS}}\rangle$ depends on the true neutrino mass, being undefined if $m_\nu^2 < 0$. Second, while negative values of m_ν^2 are called for in neutrino mass analyses to account for a possible rate overshoot near the endpoint (see [8]), such an overflow is still best explained with a positive (physical) neutrino capture signal.

KNM1 results – We perform a global fit over the analysis range $[E_0 - 37\,\mathrm{eV}, \ E_0 + 49\,\mathrm{eV}]$, treating A_{s}, E_0, m_ν^2, R_{bg} and η as free fit parameters. The covariance matrix approach is applied to propagate systematic uncertainties in the final result in exactly the same way as described in [8]. The minimization of χ^2 yields a goodness of fit with a χ^2 per degree of freedom of 0.81, reflecting a p-value of 0.71. The best fit value for $m_\nu^2 = 0.8 \pm 0.8$ eV^2 is consistent with the value obtained in the neutrino mass analysis [8]. Concerning the main observable η, we obtain a best fit value of $(3.7 \pm 1.4) \cdot 10^{11}$ with an uncertainty fully dominated by statistics. This fit is displayed by the red line in the top panel of Fig. 5. The $(\Delta\chi^2)_{\mathrm{0H}}$ between the best fit and the null hypothesis ($\eta \approx 0$) is 3.7. On the basis of 1000 simulated pseudo-experiments, the probability of obtaining $\eta \geq 3.7 \cdot 10^{11}$ if the null hypothesis (0H) is true is 2%. We therefore conclude that our result does not provide evidence for a relic neutrino signal. To obtain the η exclusion contour, we first perform a scan over both m_ν^2 and η ranging over $[0\,\mathrm{eV}^2, 1\,\mathrm{eV}^2]$ and $[0, 8.5 \cdot 10^{11}]$ re-

spectively. For each fixed pair of m_ν^2 and η, we perform the fit of the spectrum marginalizing over the remaining free fit parameters $A_{\rm s}$, E_0 and $R_{\rm bg}$. When accounting for the positive best fit on the data, the resulting 99% C.L. exclusion limit shown in Figure 6 is in good agreement with our simulations based on the same full analysis performed on a Monte Carlo copy of the data (99% sensitivity: $\eta < 4.5 \cdot 10^{11}$).
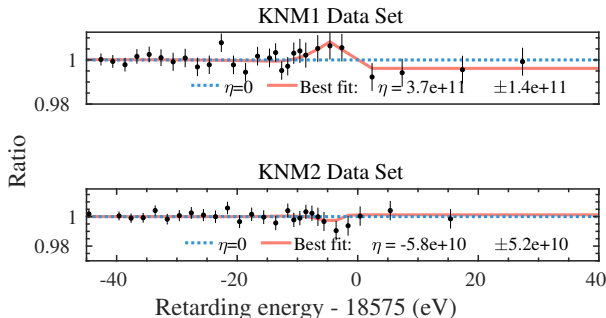

FIG. 5. Spectral ratio of the best fits for relic neutrinos with respect to the null hypothesis, $\eta = 0$, top) for the first and bottom) for the second measurement campaigns. The non-zero values of the best fit of η are both consistent with background fluctuations.

KNM2 results – This analysis is identical in all respects to the KNM1 case, except for a slightly different set of systematic effects, as described in detail in [7]. The fit of both the β spectrum and the CνB signal over the analysis range $[E_0 - 40\,{\rm eV},\ E_0 + 135\,{\rm eV}]$ leads to a χ^2 per degree of freedom of 1.15, corresponding to a p-value of 0.28. We obtain a best fit value of $\eta = (-5.8 \pm 5.2) \cdot 10^{10}$, shown by the red line in the bottom panel of Fig. 5, and $m_\nu^2 = 0.1 \pm 0.3\,{\rm eV}^2$ in agreement with [7]. Again, the uncertainty on η is fully driven by statistics. The value of $\left(\Delta\chi^2\right)_{\rm 0H}$ is found to be 1.1. Using 1000 simulated pseudo-experiments mimicking this specific data set, we determine a 5% probability of obtaining $\eta \leq -5.8 \cdot 10^{10}$ considering the null hypothesis. As for KNM1, this result is compliant with the null hypothesis and no evidence for a relic neutrino signal arises. The exclusion limit for the parameter η is obtained in the same way as for KNM1 (explained above), and the resulting 99% C.L. exclusion contour is shown in Fig. 6. The contour is computed with respect to the null hypothesis so as not to benefit from the non-physical best fit related to negative overdensity. The resulting contours are in good agreement with our simulations, both for our main limit, and for the raster scan method also performed for KNM2 (99% sensitivity: $\eta < 1.8 \cdot 10^{11}$).

Combination of individual results – We combine the results of KNM1 and KNM2 to obtain a final result with the full 2019 KATRIN data set. Since the uncertainties of KNM1 and KNM2 are still largely statistically dominated, we can safely presume that the correlations between the two analyses are negligible. The two fit

parameters m_ν^2 and η are common between the data sets. Since we analyze these two parameters individually for both data sets, we can combine the analyses by adding the χ^2 surfaces on m_ν^2 and η together. We obtain a minimal χ^2 of 50.7 for 50 degrees of freedom at $(m_\nu^2, \eta) = (0.02\,{\rm eV}^2, -2.4 \cdot 10^{10})$. The resulting 99% C.L. exclusion contour, provided relative to the null hypothesis, is shown in Fig. 6. The combined upper bound is slightly higher than the result from KNM2 alone, owing to the mild positive fluctuation on η found in the KNM1 data set.
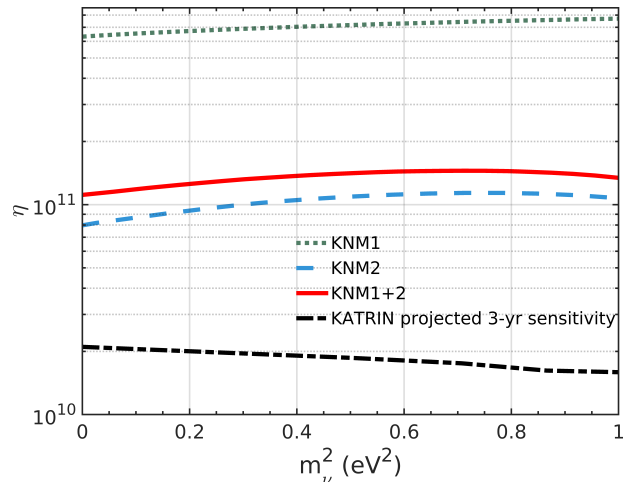

FIG. 6. Exclusion contours on the relic neutrino overdensity η at 99% C.L., for both measurement campaigns and their combination, and the projected KATRIN sensitivity for each neutrino mass.

Final sensitivity forecast – Finally, we update the sensitivity of the KATRIN experiment for the search of relic neutrinos based on the current best projection of the experimental settings [28] and using a background rate $R_{\rm bg} = 130\,{\rm mcps}$ over all 148 pixels of the detector instead of the 10 mcps design value [18]. Since the relic neutrino search is very sensitive to any background near the kinematic endpoint, the projected sensitivity is downgraded by a factor of 5 compared to the previous value in [29], to reach $\eta < 1.0 \cdot 10^{10}$ $(1.4 \cdot 10^{10},\ 1.8 \cdot 10^{10})$ at 90% (95%, 99%) C.L., which reproduces the results in [30]. Figure 7 displays an overview of existing limits on η, including our new result and the updated 3-year KATRIN sensitivity, as well as another phenomenological upper limit using the Pauli exclusion principle and the local dark matter density [31].

Conclusions and outlook – We have searched for a relic neutrino overdensity signal in data from the first two science runs of the KATRIN experiment conducted in 2019. This analysis comprises $5.16 \cdot 10^6$ β-decay electrons and $0.72 \cdot 10^6$ background events below E_0. No significant relic neutrino signal is observed and the parameter η is
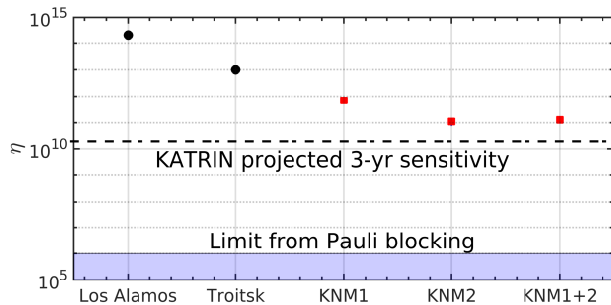
FIG. 7. Overview of the new KATRIN limits on the local relic neutrino overdensity, compared to constraints from previous experiments at Los Alamos [6] and Troitsk [5].

shown to be less than $9.7 \cdot 10^{10}$ $(1.1 \cdot 10^{11}, 1.3 \cdot 10^{11})$ at 90% (95%, 99%) for neutrino masses below 1 eV, which corresponds to an equivalent number of counts of less than $3.2 \cdot 10^4$ across both data sets. Our result improves on the previous upper limits set by direct kinematics experiments at Los Alamos [6] and Troitsk [5]. We have also highlighted that any kinematic experiment searching for the CνB via neutrino capture using a molecular source suffers from an irreducible background of rare high-energy electrons that are not involved in the energy losses associated with molecular excitations. In the case of tritium, this irreducible background overwhelms the expected CνB signal considering effective neutrino masses lower than 0.85 eV. Finally, KATRIN continues to operate toward the goal of 1000 days of data collected by 2024. The actual elevated background measurements triggered a reassessment of the final sensitivity on the relic neutrino overdensity η. We provide an updated sensitivity forecast of $\eta < 1.0 \cdot 10^{10}$ $(1.4 \cdot 10^{10}, 1.8 \cdot 10^{10})$ at 90% (95%, 99%) for a background rate of 130 mcps across all detector pixels. The PTOLEMY collaboration plans for further improvements in the future [32].

[1] A. Ringwald, (2005), arXiv:hep-ph/0505024 [hep-ph].
[2] P. de Salas, S. Gariazzo, J. Lesgourgues, and S. Pastor, Journal of Cosmology and Astroparticle Physics **2017** (09), 034.
[3] S. Weinberg, Phys. Rev. **128**, 1457 (1962).
[4] A. Faessler et al., International Journal of Modern Physics E **26**, 1740008 (2017).
[5] V. Lobashev et al., Nuclear Physics B - Proceedings Supplements **77**, 327 (1999).
[6] R. G. H. Robertson, T. J. Bowles, G. J. Stephenson, D. L. Wark, J. F. Wilkerson, and D. A. Knapp, Phys. Rev. Lett. **67**, 957 (1991).
[7] M. Aker et al. (KATRIN), (2021), arXiv:2105.08533 [hep-ex].
[8] M. Aker et al. (KATRIN), Phys. Rev. Lett. **123**, 221802 (2019).
[9] M. Aker et al. (KATRIN), Physical Review Letters **126** (2021).
[10] V. M. Lobashev and P. E. Spivak, Nucl. Instrum. Methods A **240**, 305 (1985).
[11] A. Picard et al., Nucl. Instrum. Methods Phys. Res. B **63**, 345 (1992).
[12] C. Kraus et al., Eur. Phys. J. C **40**, 447 (2005).
[13] V. N. Aseev et al., Phys. Rev. D **84**, 112003 (2011).
[14] F. Priester, M. Sturm, and B. Bornschein, Vacuum **116**, 42 (2015).
[15] A. Osipowicz et al. (KATRIN), (2001), arXiv:hep-ex/0109033.
[16] M. Arenz et al. (KATRIN), JINST **13** (08), T08005.
[17] J. F. Amsbaugh et al., Nucl. Instrum. Methods Phys. Res. A **778**, 40 (2015).
[18] J. Angrik et al. (KATRIN), FZKA scientific report , 1 (2005).
[19] M. Arenz et al. (KATRIN), JINST **13** (04), P04020.
[20] M. Arenz et al. (KATRIN), Eur. Phys. J. C **78**, 368 (2018).
[21] F. Fränkle, L. Bornschein, G. Drexlin, F. Glück, S. Görhardt, W. Käfer, S. Mertens, N. Wandkowsky, and J. Wolf, Astroparticle Physics **35**, 128 (2011).
[22] M. Arenz et al. (KATRIN), JINST **11** (04), P04011.
[23] M. Kleesiek et al., The European Physical Journal C **79** (2019).
[24] A. Saenz, S. Jonsell, and P. Froelich, Phys. Rev. Lett. **84**, 242 (2000).
[25] L. I. Bodine, D. S. Parno, and R. G. H. Robertson, Phys. Rev. C **91**, 035505 (2015).
[26] R. Hodak et al., (2011), arXiv:1102.1799 [hep-ph].
[27] Y. Cheipesh, V. Cheianov, and A. Boyarsky, (2021),

arXiv:2101.10069 [hep-ph].

[28] M. Aker *et al.* (KATRIN), Journal of Instrumentation **16** (08), T08015.

[29] A. Kaboth, J. A. Formaggio, and B. Monreal, Physical Review D **82** (2010).

[30] F. Heizmann, Ph.D. thesis, Karlsruher Institut für Tech-

nologie (KIT) (2019).

[31] J. I. Read, Journal of Physics G: Nuclear and Particle Physics **41**, 063101 (2014).

[32] E. Baracchini *et al.* (PTOLEMY), (2018), arXiv:1808.01892 [physics.ins-det].